

Spin states and persistent currents in mesoscopic rings: spin-orbit interactions

J. S. Sheng and Kai Chang*

SKLSM, Institute of Semiconductors, Chinese Academy of Sciences, P. O. Box 912, Beijing 100083, China

We investigate theoretically electron spin states in one dimensional (1D) and two dimensional (2D) hard-wall mesoscopic rings in the presence of both the Rashba spin-orbit interaction (RSOI) and the Dresselhaus spin-orbit interaction (DSOI) in a perpendicular magnetic field. The Hamiltonian of the RSOI alone is mathematically equivalent to that of the DSOI alone using an $SU(2)$ spin rotation transformation. Our theoretical results show that the interplay between the RSOI and DSOI results in an effective periodic potential, which consequently leads to gaps in the energy spectrum. This periodic potential also weakens and smoothens the oscillations of the persistent charge current (CC) and spin current (SC) and results in the localization of electrons. For a 2D ring with a finite width, higher radial modes destroy the periodic oscillations of persistent currents.

PACS numbers: 73.23.Ra, 71.70.Ej, 72.25.Dc

I. INTRODUCTION

In recent years, the spin-orbit interaction (SOI) in low-dimensional semiconductor structures has attracted considerable attention due to its potential applications in spintronic devices.^{1,2} There are two types of SOI in conventional semiconductors. One is the Dresselhaus spin-orbit interaction (DSOI) induced by bulk inversion asymmetry,³ and the other is the Rashba spin-orbit interaction (RSOI) induced by structure inversion asymmetry.^{4,5} The strength of the RSOI can be tuned by external gate voltages or asymmetric doping. Recently, the intrinsic spin Hall effect (SHE) in a spin-orbit coupled three-dimensional p-doped semiconductor⁶ and in a Rashba spin-orbit coupled two-dimensional electron system⁷ was predicted theoretically. It provides us a possibility to generate the spin current (SC) electrically without the use of ferromagnetic metal or a magnetic field.

Recently advanced growth techniques make it possible to fabricate high quality semiconductor rings.⁸ A quantum ring exhibits the intriguing spin interference phenomenon because of its unique topology. The persistent CC in mesoscopic rings threaded by a magnetic $U(1)$ flux has been studied extensively, neglecting the spin degree of freedom of the electron.^{9,10,11} It has been experimentally observed both in a gold ring¹² and in a GaAs-AlGaAs ring¹³ using standard SQUID magnetometry. As for the persistent SC, the SC-induced electric field that was predicted by several authors^{14,15} may contribute to the successful measurement of the persistent SC in mesoscopic rings in future. The electronic structures and magneto-transport properties of 1D rings with the RSOI alone have attracted considerable interest.^{16,17,18} Since the strength of the DSOI in thin quantum wells is comparable with that of the RSOI,¹⁹ one should consider both of the SOI's in low dimensional structures. A few works have been done on the effects of the competition between these two types of SOI on the transport properties of 2DEG.^{20,21,22} The effects of the interplay between the RSOI and DSOI on the spin states and persistent

currents (CC and SC) in mesoscopic rings are highly desirable.

In this paper, we investigate theoretically the spin states and persistent CC and SC in mesoscopic rings under a uniform perpendicular magnetic field in the presence of both RSOI and DSOI. We find that the persistent CC and SC, charge density distribution, and local spin orientation are very sensitive to the strength of the RSOI and DSOI. The interplay between the RSOI and DSOI leads to an effective periodic potential. This potential has significant effects on the physical properties of mesoscopic rings, e.g., the energy gaps, the localization of electrons, and weakening and smoothing of persistent CC and SC. Five different cases are considered: (1) a 1D ring with RSOI alone; (2) a 1D ring with DSOI alone; (3) a 1D ring with RSOI and DSOI of equal strengths; (4) a 1D ring with RSOI and DSOI of different strengths; (5) finite-width effects on the energy spectrum, charge density distribution, the persistent CC and SC. The eigenstates of cases one and two are analytically solved and can be connected by a unitary transformation. The paper is organized as follows. In Sec. II the theoretical model is presented. The numerical results and discussions are given in Sec. III. Finally, we give a brief conclusion in Sec. IV.

II. THEORETICAL MODEL

A. Hamiltonian

In the presence of both RSOI and DSOI, the single-particle Hamiltonian for an electron in a finite-width ring (see Fig. 1(b)) under a uniform perpendicular magnetic field reads

$$H = \frac{\hbar^2 k^2}{2m^*} + \alpha(\sigma_x k_y - \sigma_y k_x) + \beta(\sigma_x k_x - \sigma_y k_y) + \frac{1}{2}g^* \mu_B B \sigma_z + V(r), \quad (1)$$

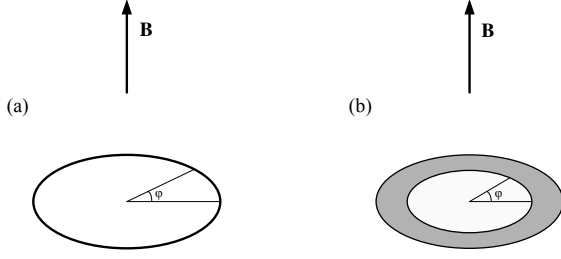


FIG. 1: Schematic diagrams for 1D ideal ring (a) and 2D hard-wall ring (b).

where $\mathbf{k} = -i\nabla + e\mathbf{A}/\hbar$. $\mathbf{A}(\mathbf{r}) = B/2(-y, x, 0)$ is the vector potential. m^* is the electron effective mass. The fourth term describes the Zeeman splitting with Bohr magneton $\mu_B = e\hbar/2m_e$ and the effective g factor g^* . σ_i ($i = x, y, z$) are the Pauli matrices. α and β specify the RSOI and DSOI strengths, respectively. $V(r)$ is the radial confining potential,

$$V(r) = \begin{cases} 0 & r_1 \leq r \leq r_2 \\ \infty & \text{otherwise} \end{cases}, \quad (2)$$

where r_1 and r_2 are the inner and outer radii of the ring, respectively.

In the following we take the average radius $a = (r_1 + r_2)/2$ as the length unit and $E_0 = \hbar^2/2m^*a^2$ as the energy unit. The dimensionless Hamiltonian in the polar coordinates becomes

$$H = \begin{bmatrix} H_k + V(r) + \bar{g}b/2 & \bar{\beta}k_+ + i\bar{\alpha}k_- \\ \bar{\beta}k_- - i\bar{\alpha}k_+ & H_k + V(r) - \bar{g}b/2 \end{bmatrix}, \quad (3)$$

where $H_k = (\mathbf{e}_r k_r + \mathbf{e}_\varphi k_\varphi)^2$ is the dimensionless kinetic term; $k_\pm = k_x \pm ik_y = e^{\pm i\varphi}(k_r \pm ik_\varphi)$, with $k_r = -i\frac{\partial}{\partial r}$ and $k_\varphi = -\frac{i}{r}\frac{\partial}{\partial \varphi} + \frac{b}{4}r$; $b = \hbar eB/m^*E_0$ is the dimensionless magnetic field; $\bar{\alpha}(\bar{\beta}) = \alpha(\beta)/E_0a$ specifies the dimensionless RSOI (DSOI) strength; and $\bar{g} = g^*m^*/2m_e$ is the dimensionless g factor.

The wavefunction $\Psi(\mathbf{r})$ of an electron in the ring can be expanded as

$$\Psi(\mathbf{r}) = \sum_{nm\sigma} a_{nm\sigma} R_n(r) \Theta_m(\varphi) \chi_\sigma(s_z), \quad (4)$$

$$R_n(r) \Theta_m(\varphi) \chi_\sigma(s_z) = \sqrt{\frac{2}{dr}} \sin\left[\frac{n\pi}{d}(r - r_1)\right] \cdot \frac{1}{\sqrt{2\pi}} e^{im\varphi} \cdot \chi_\sigma(s_z), \quad (5)$$

where $d = r_2 - r_1$ is the width of the ring and $\chi_\sigma(s_z)$ ($\sigma = \pm 1$) are the eigenvectors of s_z .

Most previous theoretical studies on mesoscopic rings are based on the Hamiltonian of a 1D ring (see Fig. 1(a)), which can be obtained by simply disregarding all the terms proportional to derivatives with respect to r in the 2D Hamiltonian. But this conventional procedure

leads to a non-hermitian Hamiltonian in the presence of RSOI or DSOI.²³ We can obtain a hermitian Hamiltonian including both RSOI and DSOI following Ref. 23. The stationary Schrödinger equation is

$$H\Psi = E\Psi. \quad (6)$$

The dimensionless 1D Hamiltonian including both RSOI and DSOI reads

$$H = \left[-i\frac{\partial}{\partial \varphi} + \frac{\Phi}{\Phi_0} + \frac{\bar{\alpha}}{2}\sigma_r - \frac{\bar{\beta}}{2}\sigma_\varphi(-\varphi) \right]^2 - \frac{\bar{\alpha}^2 + \bar{\beta}^2}{4} + \frac{\bar{\alpha}\bar{\beta}}{2}\sin 2\varphi + \frac{1}{2}\bar{g}b\sigma_z, \quad (7)$$

where $\sigma_r = \cos\varphi\sigma_x + \sin\varphi\sigma_y$, $\sigma_\varphi = \cos\varphi\sigma_y - \sin\varphi\sigma_x$, $\Phi = B\pi a^2$ is the magnetic flux threading the ring, and $\Phi_0 = h/e$ is the flux unit. Notice that there is a periodic potential term ($\frac{\bar{\alpha}\bar{\beta}}{2}\sin 2\varphi$) induced by the interplay between the RSOI and DSOI.

We introduce a vector function $S(\mathbf{r})$ to describe the local spin orientation of a specific eigenstate Ψ in a 1D ring:

$$S(\mathbf{r}) = \Psi^\dagger \mathbf{s} \Psi = \Psi^\dagger s_x \Psi \mathbf{e}_x + \Psi^\dagger s_y \Psi \mathbf{e}_y + \Psi^\dagger s_z \Psi \mathbf{e}_z. \quad (8)$$

When the coupling strength $\bar{\alpha}$ or $\bar{\beta}$ vanishes, the $\sin 2\varphi$ potential accordingly disappears and the analytical solution to the eigenvalue problem is available (see Appendix for details). Generally we have to solve Eq. (6) numerically when $\bar{\alpha} \neq 0$ and $\bar{\beta} \neq 0$.

B. Persistent currents

The charge density operator and the charge current density operator are

$$\hat{\rho}(\mathbf{r}') = -e\delta(\mathbf{r}' - \mathbf{r}) \\ \hat{j}_c(\mathbf{r}') = \frac{1}{2}[\hat{\rho}(\mathbf{r}')\hat{\mathbf{v}} + \hat{\mathbf{v}}\hat{\rho}(\mathbf{r}')], \quad (9)$$

where \mathbf{r}' refers to the field coordinates and \mathbf{r} the coordinates of the electron. We can also introduce the spin density operator and spin current density operator¹⁶ as

$$\hat{S}(\mathbf{r}') = \frac{\hbar}{2}\hat{\boldsymbol{\sigma}}\delta(\mathbf{r}' - \mathbf{r}) \\ \hat{j}_s(\mathbf{r}') = \frac{1}{2}[\hat{S}(\mathbf{r}')\hat{\mathbf{v}} + \hat{\mathbf{v}}\hat{S}(\mathbf{r}')], \quad (10)$$

where $\hat{\boldsymbol{\sigma}} = \hat{\sigma}_x \mathbf{e}_x + \hat{\sigma}_y \mathbf{e}_y + \hat{\sigma}_z \mathbf{e}_z$ is the vector of the Pauli matrices. The charge current density and spin current density can be obtained by calculating the expectation values of the corresponding operators:

$$\mathbf{j}_c(\mathbf{r}') = \langle \Psi | \hat{j}_c | \Psi \rangle = -e \text{Re} \{ \Psi^\dagger(\mathbf{r}') \hat{\mathbf{v}}' \Psi(\mathbf{r}') \} \\ \mathbf{j}_s(\mathbf{r}') = \langle \Psi | \hat{j}_s | \Psi \rangle = \text{Re} \{ \Psi^\dagger(\mathbf{r}') \hat{\mathbf{v}}' \hat{S}(\mathbf{r}') \Psi(\mathbf{r}') \}, \quad (11)$$

TABLE I: Parameters used in our calculation are from Ref. 26.

	$m^*(m_e)$	g^*
GaAs	0.067	-0.44
InSb	0.014	-51

where $\Psi(\mathbf{r})$ is the wavefunction of an electron in the ring. For convenience, we note \mathbf{r}' , $\hat{\mathbf{v}}'$ as \mathbf{r} , $\hat{\mathbf{v}}$ hereafter.

The φ -component of the velocity operator associated with the Hamiltonian in Eq. (1) is

$$\hat{v}_\varphi = \mathbf{e}_\varphi \left[\frac{\hbar}{im^*r} \frac{\partial}{\partial \varphi} + \frac{eBr}{2m^*} + \frac{\alpha}{\hbar} \sigma_r - \frac{\beta}{\hbar} \sigma_\varphi(-\varphi) \right]. \quad (12)$$

The azimuthal (spin or charge) current can be defined as¹⁰

$$I_\varphi = \frac{1}{2\pi} \int_0^{2\pi} d\varphi \int_{r_1}^{r_2} dr j_\varphi(\mathbf{r}). \quad (13)$$

We ignore the Coulomb interaction between electrons in this work. At the low temperature, N electrons will occupy the lowest N levels of the energy spectrum. The total (charge or spin) current is the summation over all occupied levels.¹⁶

For a 1D ring, the eigenstates could be expanded in the basis set $\Theta_m(\varphi) = \exp(im\varphi)/\sqrt{2\pi}$ which is much simpler than that in Eq. (4), and we can get the azimuthal component of the velocity operator in a 1D ring by specifying the variable r as the constant a in Eq. (12).

Most of the previous investigations of the persistent CC in mesoscopic rings are based on the well-known formula $I_n = -\partial E_n / \partial \Phi$, where I_n denotes the contribution to the persistent CC from the n th state and Φ is the magnetic flux through the ring.^{16,24,25} In this paper we calculate the persistent CC and SC via Eq. (11). Note that for a 1D ring our results are identical with those obtained from the formula $I_n = -\partial E_n / \partial \Phi$.

III. RESULTS AND DISCUSSION

We show the energy spectrum of a 1D ring in Fig. 2 for different g factors. The relevant parameters of the materials used in our calculation are listed in Table I. Without the spin-orbit couplings, the g factor accounts for the spin splitting. For a material with large g factor such as InSb, although the parabola behavior of the energy levels as functions of the magnetic fields is still retained, the periodicity of the energy spectrum is severely broken by the g factor, especially at large magnetic fields. For a material with a small g factor, e.g. GaAs, the Zeeman splitting is quite small even in a rather large magnetic field.

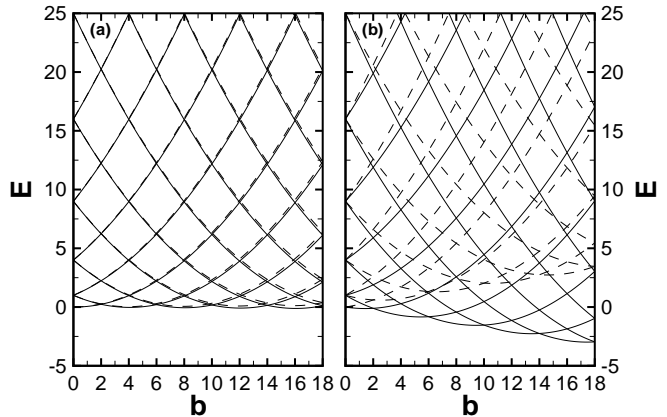


FIG. 2: (a) The energy spectrum for 1D GaAs rings. $\bar{\alpha} = \bar{\beta} = 0$, $\bar{g} = -0.01474$; (b) The energy spectrum for 1D InSb ring. $\bar{\alpha} = \bar{\beta} = 0$, $\bar{g} = -0.357$. In Fig. 2(a) and Fig. 2(b) the solid (dashed) lines denote spin-up (spin-down) levels.

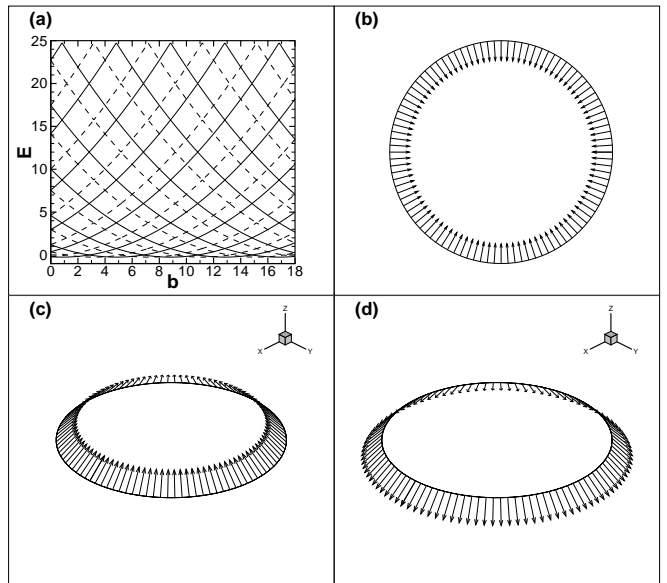


FIG. 3: (a) Energy spectrum of 1D ring in the presence of RSOI alone, where the solid lines (dashed lines) denote the spin-up (spin-down) levels; (b) The projection of $S(\mathbf{r})_{\uparrow}^R$ onto the x - y plane; (c) Local spin orientation for all the spin-up levels $S(\mathbf{r})_{\uparrow}^R$; (d) Local spin orientation for all the spin-down levels $S(\mathbf{r})_{\downarrow}^R$. $\bar{\alpha} = 1$, $\bar{\beta} = 0$ and $\bar{g} = 0$.

A. 1D ring with RSOI alone

As shown in the Appendix, the electron states in a 1D ring with RSOI alone under a uniform magnetic field including the Zeeman splitting can be solved analytically.

The energy spectrum in the presence of RSOI alone is plotted in Fig. 3(a). When the g factor is set to be zero,

the energy of each level is given by

$$E_{n,\sigma} = \left(n + \frac{b}{4} + \frac{\sigma}{2} - \frac{\sigma}{2 \cos \theta} \right)^2 - \frac{\tan^2 \theta}{4}, \quad (14)$$

where $\theta = \arctan(\bar{\alpha})$ (Eq. (A.11) or Eq. (A.12) represents the corresponding eigenstate so long as $\theta_{n,\sigma}$ is replaced by θ). From the above expression we find that the spin-up and spin-down levels with the same quantum number n are separated in the b axis by $4(1/\cos\theta - 1)$, and both of the spin-up and spin-down levels are pulled down by $\tan^2\theta/4$ compared to the case without SOI.

For the RSOI alone case, the local spin orientation for all the spin-up states along the ring is described as

$$\begin{aligned} S(\mathbf{r})_{\uparrow}^R &= \Psi_{n,\uparrow}^{R\dagger} s_x \Psi_{n,\uparrow}^R \mathbf{e}_x + \Psi_{n,\uparrow}^{R\dagger} s_y \Psi_{n,\uparrow}^R \mathbf{e}_y + \Psi_{n,\uparrow}^{R\dagger} s_z \Psi_{n,\uparrow}^R \mathbf{e}_z \\ &= \frac{\hbar}{4\pi a} [\sin(-\theta)(\cos\varphi \mathbf{e}_x + \sin\varphi \mathbf{e}_y) + \cos(-\theta)\mathbf{e}_z]. \end{aligned} \quad (15)$$

The local spin orientation for all the spin-down states $S(\mathbf{r})_{\downarrow}^R$ is opposite to $S(\mathbf{r})_{\uparrow}^R$ as shown in Fig. 3(c) and Fig. 3(d). In this case, the oblique angle $\theta = \arctan(\bar{\alpha})$ becomes independent from the quantum number n and the magnetic field b . It means that the local spin orientations for all the spin-up (spin-down) states are the same. When there is RSOI alone, the local spin orientation exhibits rotational symmetry for either spin-up or spin-down states.

The contributions to the persistent CC and SC from each level can be easily obtained explicitly:

$$I_{n,\sigma} = - \left(n + \frac{b}{4} + \frac{\sigma}{2} - \frac{\sigma}{2 \cos \theta} \right), \quad (16a)$$

$$I_{n,\sigma}^{s_z} = \left(n + \frac{b}{4} + \frac{\sigma}{2} - \frac{\sigma}{2 \cos \theta} \right) \sigma \cos \theta. \quad (16b)$$

$I_{n,\sigma}$ ($I_{n,\sigma}^{s_z}$) denotes the contribution to the persistent CC (SC) from the eigenstate $\Psi_{n,\sigma}$. $I_{n,\sigma}$ ($I_{n,\sigma}^{s_z}$) is in the units of $2E_0/\Phi_0$ ($E_0/2\pi$). We should notice that these expressions deduced from operators coincide with the formula $I_n = -\partial E_n/\partial\Phi$.

Splettstoesser *et al.* analyzed the persistent CC induced by the magnetic flux in the 1D ring with both RSOI and a impurity potential.¹⁶ They demonstrated that the strength of the RSOI can be extracted from the dependence of the persistent CC on the magnetic flux. The number of electrons N in their work was assumed to be large enough. We focus on the case in which there are few electrons in the ring (see Fig. 4). We find that the persistent CC is a periodic function of b exhibiting many linear segments with a slope ratio of $-1/4$ which can be easily deduced from Eq. (16a). The periodicity of the persistent CC for an arbitrary N is 4, the same as that of the energy spectrum. For an arbitrary even number of electrons $N = 2n$, the jumping amplitude is $1/2$ and the neighboring two jumps are shifted along the CC axis. For an odd number of electrons $N = 2n + 1$, there

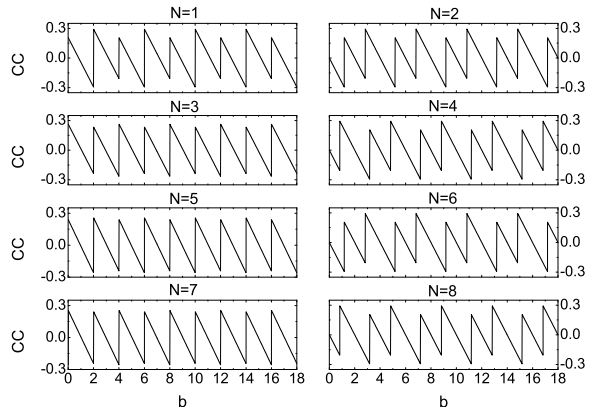


FIG. 4: The persistent CC in a 1D ring with different numbers of electrons N vs magnetic field b while $\bar{\alpha} = 1$, $\bar{\beta} = 0$, $\bar{g} = 0$. The persistent CC is in units of $2NE_0/\Phi_0$.

are two jumping amplitudes which appear alternately at those points where $b = 0, 2, 4, 6, \dots$. One jumping amplitude is $(n - 1/\cos\theta + 2)/(2n + 1)$, while the other is $(n + 1/\cos\theta - 1)/(2n + 1)$. When n approaches infinity, the above two amplitudes tend to $1/2$.

The dependence of the persistent SC on the magnetic field b shows interesting behavior. Turning (jumping) points in the persistent SC oscillation for an odd (even) number of electrons are caused by the crossing of levels with opposite (same) spins. When the magnetic field b sweeps, the persistent SC oscillation for an odd (even) number of electrons exhibits saw-tooth (square) wave behavior and the oscillation amplitude of the persistent SC for an even number of electrons is bigger than that for a neighboring odd number of electrons especially when the number of electrons increases. For an odd number of electrons $N = 2n + 1$, the slope ratios of the persistent SC are $\pm \cos\theta/4(2n + 1)$ alternately. For an even number of electrons $N = 2n$, the jumping amplitude is $\cos\theta/2$ for all jumping points.

B. 1D ring with DSOI alone

Now we consider a 1D ring with DSOI alone. The eigenstates of the Hamiltonian of a 1D ring with $\bar{\alpha} = a$, $\bar{\beta} = b$, and $\bar{g} = c$ can be connected to those with $\bar{\alpha} = b$, $\bar{\beta} = a$, and $\bar{g} = -c$ by a unitary operator T (see the Appendix). As we will show in the next subsection, T represents a rotational transformation in spin space. b and c are set to be zero and the relationship between the RSOI alone case and DSOI alone case is specified as

$$E_{n,\sigma}^D = E_{n,-\sigma}^R, \quad (17a)$$

$$\Psi_{n,\uparrow}^D = \exp[i\pi/4]T\Psi_{n,\downarrow}^R, \quad (17b)$$

$$\Psi_{n,\downarrow}^D = \exp[-i\pi/4]T^\dagger\Psi_{n,\uparrow}^R. \quad (17c)$$

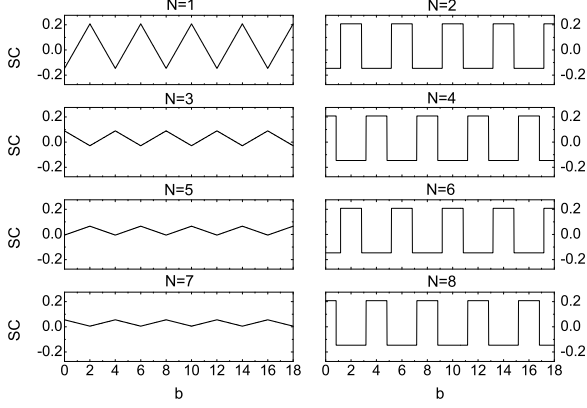


FIG. 5: Same as Fig. 4, but for the persistent SC. The persistent SC is in units of $NE_0/2\pi$.

The energy spectrum while $\bar{\alpha} = 0$, $\bar{\beta} = 1$, and $\bar{g} = 0$ is plotted in Fig. 6(a), which is exactly the same as that of a 1D ring with RSOI alone (see Fig. 3(a)), but the spin orientations of the corresponding eigenstates are different. This feature arises from the sign reversal behavior of σ_z under the unitary transformation T .

Although the eigenstates for the RSOI alone case and those for the DSOI alone case can be connected by the unitary transformation T , the behaviors of $S(\mathbf{r})_{\uparrow\downarrow}^R$ and $S(\mathbf{r})_{\uparrow\downarrow}^D$ are very different. In the case with DSOI alone, spin-up (spin-down) states with different angular quantum number n or under different magnetic field b share the same local spin orientation $S(\mathbf{r})_{\uparrow}^D$ ($S(\mathbf{r})_{\downarrow}^D$). The angle between $S(\mathbf{r})_{\uparrow}^D$ ($S(\mathbf{r})_{\downarrow}^D$) and the z -axis is $-\theta$ ($\pi - \theta$). The local spin orientations $S(\mathbf{r})_{\uparrow\downarrow}^D$ can be obtained by interchanging the x and y components of $S(\mathbf{r})_{\uparrow\downarrow}^R$ (see Eqs. (15) and (18)).

$$\begin{aligned}
S(\mathbf{r})_{\uparrow}^D &= \Psi_{n,\uparrow}^{D\dagger} s_x \Psi_{n,\uparrow}^D \mathbf{e}_x + \Psi_{n,\uparrow}^{D\dagger} s_y \Psi_{n,\uparrow}^D \mathbf{e}_y + \Psi_{n,\uparrow}^{D\dagger} s_z \Psi_{n,\uparrow}^D \mathbf{e}_z \\
&= \Psi_{n,\downarrow}^{R\dagger} T^\dagger s_x T \Psi_{n,\downarrow}^R \mathbf{e}_x + \Psi_{n,\downarrow}^{R\dagger} T^\dagger s_y T \Psi_{n,\downarrow}^R \mathbf{e}_y \\
&+ \Psi_{n,\downarrow}^{R\dagger} T^\dagger s_z T \Psi_{n,\downarrow}^R \mathbf{e}_z \\
&= -\Psi_{n,\downarrow}^{R\dagger} s_y \Psi_{n,\downarrow}^R \mathbf{e}_x - \Psi_{n,\downarrow}^{R\dagger} s_x \Psi_{n,\downarrow}^R \mathbf{e}_y - \Psi_{n,\downarrow}^{R\dagger} s_z \Psi_{n,\downarrow}^R \mathbf{e}_z \\
&= \Psi_{n,\uparrow}^{R\dagger} s_y \Psi_{n,\uparrow}^R \mathbf{e}_x + \Psi_{n,\uparrow}^{R\dagger} s_x \Psi_{n,\uparrow}^R \mathbf{e}_y + \Psi_{n,\uparrow}^{R\dagger} s_z \Psi_{n,\uparrow}^R \mathbf{e}_z \\
&= \frac{\hbar}{4\pi a} [\sin(-\theta)(\sin \varphi \mathbf{e}_x + \cos \varphi \mathbf{e}_y) + \cos(-\theta) \mathbf{e}_z]. \quad (18)
\end{aligned}$$

This interesting feature comes from the behavior of $\sigma_{x(y)}$ under the unitary transformation T , i.e., $T\sigma_{x(y)}T^\dagger = T^\dagger\sigma_{x(y)}T = -\sigma_{y(x)}$. The projections of $S(\mathbf{r})_{\uparrow}^R$ and $S(\mathbf{r})_{\uparrow}^D$ onto the x - y plane are very different (see Fig. 3(b) and Fig. 6(b)). For the RSOI alone case, the vector always points along the radial direction and the locus of the arrowhead is a circle (see Fig. 3(b)). For the DSOI alone

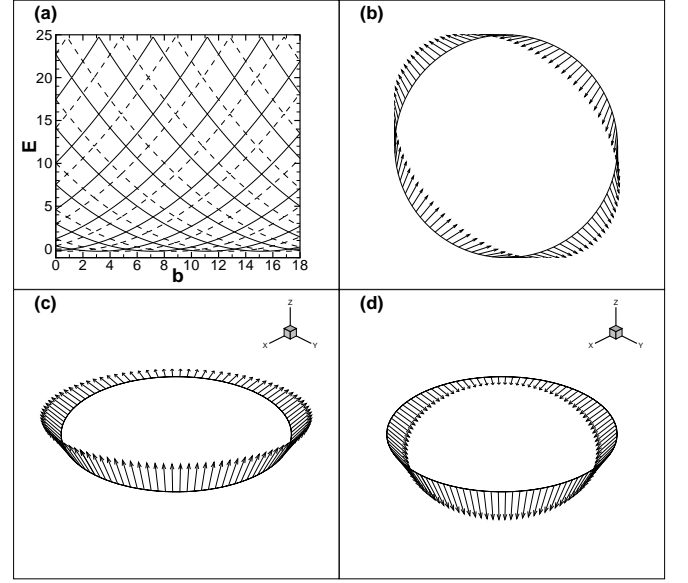


FIG. 6: (a) Energy spectrum of 1D ring in the presence of DSOI alone, where the solid lines (dashed lines) denote the spin-up (spin-down) levels; (b) The projection of $S(\mathbf{r})_{\uparrow}^D$ onto the x - y plane; (c) Local spin orientation for all the spin-up levels $S(\mathbf{r})_{\uparrow}^D$; (d) Local spin orientation for all the spin-down levels $S(\mathbf{r})_{\downarrow}^D$. $\bar{\alpha} = 0$, $\bar{\beta} = 1$ and $\bar{g} = 0$.

case, the vector varies along the ring and the cylindrical symmetry is broken (see Fig. 6(b)).

In the current case, the persistent CC oscillations exhibit the same behavior as those of the RSOI alone case (see Fig. 4) because the corresponding levels are identical as functions of the magnetic field b . We know that the contribution of each level to the persistent SC is related not only to the magnetic field dependence of the eigenenergy but also to the spin orientation of the eigenstate. Since the spin-up and spin-down levels are interchanged compared to those of the RSOI alone case, the persistent SC in the current case can be obtained by changing the sign of the persistent SC for the RSOI alone case.

C. 1D ring with equal strength RSOI and DSOI

The electron energy spectra for $\bar{\alpha} = \bar{\beta} = 1$, $\bar{g} = 0$ and $\bar{\alpha} = \bar{\beta} = 3$, $\bar{g} = 0$ are plotted in Figs. 7(a) and 7(c), respectively. We can see that the energy spectra are spin degenerate. The spin degeneracy comes from the symmetry of the Hamiltonian when $\bar{\alpha} = \bar{\beta}$. In this paper, we use the unitary operator T (see Appendix) to describe the symmetry of the 1D Hamiltonian. When $\bar{\alpha} = \bar{\beta} \neq 0$ and $\bar{g} = 0$, $THT^\dagger = T^\dagger HT = H$. If we have $H\Psi = E\Psi$, in which Ψ is an eigenstate for the eigenenergy E , then the states $T\Psi$ and $T^\dagger\Psi$ are also eigenstates and are equivalent to each other. Thus the energy levels are twofold degenerate. The operator for a φ rotation around

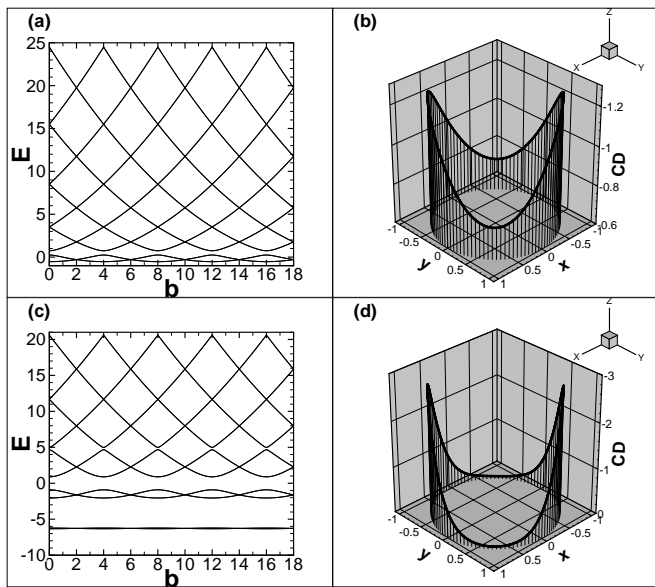


FIG. 7: (a) Energy spectrum of 1D ring while $\bar{\alpha} = \bar{\beta} = 1$, $\bar{g} = 0$; (b) The charge density (CD) distribution of the lowest single electron state in a 1D ring while $\bar{\alpha} = \bar{\beta} = 1$, $\bar{g} = 0$, $b = 0$; (c) Energy spectrum of 1D ring while $\bar{\alpha} = \bar{\beta} = 3$, $\bar{g} = 0$; (d) The charge density (CD) distribution of the lowest single electron state in a 1D ring while $\bar{\alpha} = \bar{\beta} = 3$, $\bar{g} = 0$, $b = 0$. The charge density is in units of $e/2\pi a$.

the unit vector \mathbf{n} in the Hilbert space reads

$$D(\mathbf{n}, \varphi) = e^{-i\varphi \mathbf{n} \cdot \mathbf{L}/\hbar} \otimes e^{-i\varphi \mathbf{n} \cdot \mathbf{s}/\hbar}, \quad (19)$$

where \mathbf{L} and \mathbf{s} denote the orbital and spin angular momentum operators, respectively. It is easy to demonstrate that the unitary operator T can be written as $\exp[-i\pi \mathbf{n}_1 \cdot \mathbf{s}/\hbar]$ with $\mathbf{n}_1 = (1/\sqrt{2}, -1/\sqrt{2}, 0)$. Then T is actually a rotation operator in the spin space. For a quantum ring in the x - y plane, the orbital angular momentum vector $\mathbf{L} = \mathbf{r} \times \mathbf{p}$ points along the z -axis, and therefore $\mathbf{n}_1 \cdot \mathbf{L} = 0$. Thus the unitary operator T is eventually a rotation operator in the whole Hilbert space:

$$T = D(\mathbf{n}_1, \pi). \quad (20)$$

That means the unitary transformation T (T^\dagger) is actually a rotation by π ($-\pi$) around \mathbf{n}_1 . Similarly, there are also symmetric operations corresponding to π and $-\pi$ rotations around $\mathbf{n}_2 = (1/\sqrt{2}, 1/\sqrt{2}, 0)$ for the Hamiltonian with $\bar{\alpha} = -\bar{\beta}$. We need to stress that these symmetric operations also exist for a two-dimensional electron gas with equal strength RSOI and DSOI ($\bar{\alpha} = \pm\bar{\beta}$) and $\bar{g} = 0$.

Besides the spin degeneracy, it is interesting to find that gaps appear in the energy spectra. In order to understand this feature, we transform the original Hamiltonian to a simple form via a unitary transformation A

as follows:

$$A = \frac{1}{\sqrt{2}} \cdot \begin{bmatrix} \exp[-i\bar{\alpha}f(\varphi)] & \exp[i\bar{\alpha}f(\varphi)] \\ \exp[-i\pi/4] \exp[-i\bar{\alpha}f(\varphi)] & -\exp[-i\pi/4] \exp[i\bar{\alpha}f(\varphi)] \end{bmatrix}, \quad (21)$$

with $f(\varphi) = \sin(\varphi + \pi/4)$. The original electron Hamiltonian with $\bar{\alpha} = \bar{\beta}$ and $\bar{g} = 0$ reads

$$H = \left[-i \frac{\partial}{\partial \varphi} + \frac{b}{4} + \frac{\bar{\alpha}}{2} \sigma_r - \frac{\bar{\alpha}}{2} \sigma_\varphi(-\varphi) \right]^2 - \frac{\bar{\alpha}^2}{2} + \frac{\bar{\alpha}^2}{2} \sin 2\varphi. \quad (22)$$

After the transformation, the Hamiltonian becomes

$$H' = A^\dagger H A = \left(-i \frac{\partial}{\partial \varphi} + \frac{b}{4} \right)^2 - \frac{\bar{\alpha}^2}{2} + \frac{\bar{\alpha}^2}{2} \sin 2\varphi. \quad (23)$$

That means the Hamiltonian of a 1D ring with equal strength RSOI and DSOI and zero g factor is equivalent to that of a 1D ring with a periodic potential alone (see the last term in Eq. (23)). The potential height is proportional to the square of the SOI strength, and the average of the potential shifts down by about $\bar{\alpha}^2/2$. The eigenvectors of Eq. (23) are actually the periodic solutions of the Mathieu equation.²⁷ The energy gaps, which are proportional to the potential height, decrease with decreasing SOI strengths, especially for higher gaps (see Fig. 7(a)). When the strengths of SOI are fixed, the higher energy gaps are narrower than the lower ones because there is less influence from the potential.

When only one type of SOI (RSOI or DSOI) exists, the charge density distribution will be constant along the ring. But the charge density distribution becomes localized along the ring when both RSOI and DSOI are taken into account. This localization arises from the effective periodic potential, whose height is determined by the product of the strengths of RSOI and DSOI (see Eq. (7)). Therefore large SOI strengths lead to strong electron localization. The absolute value of the charge density exhibits maxima at the valleys of the $\sin 2\varphi$ potential ($\varphi = 3\pi/4$ or $\varphi = 7\pi/4$) and minima at the peaks of the $\sin 2\varphi$ potential ($\varphi = \pi/4$ or $\varphi = 5\pi/4$) (see Fig. 7(b) and Fig. 7(d)).

In the spin degenerate case, we cannot define the local spin orientation $S(\mathbf{r})$ for an eigenenergy level and the persistent SC for an odd number of electrons because of the uncertainty of the eigenvectors. The persistent CC oscillation for an odd number of electrons $N = 2m + 1$ is simply the arithmetic average of that for $N = 2m$ and that for $N = 2m + 2$ in a spin degenerate case. Thus we compare the persistent current (CC and SC) oscillations in the three degenerate cases: $\bar{\alpha} = \bar{\beta} = 0$, $\bar{\alpha} = \bar{\beta} = 1$, and $\bar{\alpha} = \bar{\beta} = 3$ only for even numbers of electrons (see Fig. 8). The persistent SC is zero in the two degenerate cases for even numbers of electrons. The $\sin 2\varphi$ potential

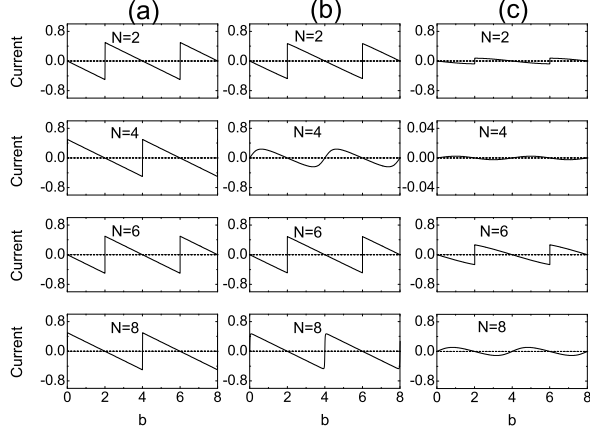


FIG. 8: The persistent CC (solid lines) and SC (dashed lines) with different even numbers of electrons N vs magnetic field in the degenerate cases (a) $\bar{\alpha} = \bar{\beta} = \bar{g} = 0$; (b) $\bar{\alpha} = \bar{\beta} = 1$, $\bar{g} = 0$; (c) $\bar{\alpha} = \bar{\beta} = 3$, $\bar{g} = 0$. The persistent CC (SC) is in units of $2NE_0/\Phi_0$ ($NE_0/2\pi$).

in Eq. (7) accounts for the flatter magnetic dispersion as well as gaps in the energy spectrum when $\bar{\alpha} = \bar{\beta} \neq 0$. Since the contribution to the persistent CC from an energy level is actually determined by the dependence of the energy level on magnetic field, the oscillation of the persistent CC for the case $\bar{\alpha} = \bar{\beta} \neq 0$ is smoother and smaller than that for the case $\bar{\alpha} = \bar{\beta} = 0$. The interplay between the RSOI and DSOI smoothens and weakens the persistent CC oscillation most obviously when the Fermi level locates near the lowest gap (see the panels labeled $N = 4$ in Fig. 8(b) and Fig. 8(c)). While the number of electrons increases, the oscillation of the persistent CC becomes sharp again since the higher gaps become smaller. This smoothing and weakening effect can even be found again for a large number of electrons when the SOI strengths increase (see Fig. 8(c)).

D. 1D ring with different strength RSOI and DSOI

Generally, the symmetry of the Hamiltonian shown in the previous subsection no longer exists when $|\bar{\alpha}| \neq |\bar{\beta}|$, even for $\bar{g} = 0$. We show the electron spectra for $\bar{\alpha} = 2$, $\bar{\beta} = 1$, $\bar{g} = 0$ and $\bar{\alpha} = 4$, $\bar{\beta} = 3$, $\bar{g} = 0$ in Fig. 9(a) and Fig. 9(c), respectively. The energy gaps increase with increasing SOI strengths. But the spin splitting in the two spectra is quite different. It is interesting to note that the energy spectrum becomes spin degenerate again when the two SOI strengths are tuned to proper values even though they are different. Figs. 9(b) and 9(d) show the distribution of charge density for different strength RSOI and DSOI. The electron is localized along the ring due to the periodic potential $\frac{\bar{\alpha}\bar{\beta}}{2} \sin 2\varphi$. The electron density distribution becomes more localized with increased potential

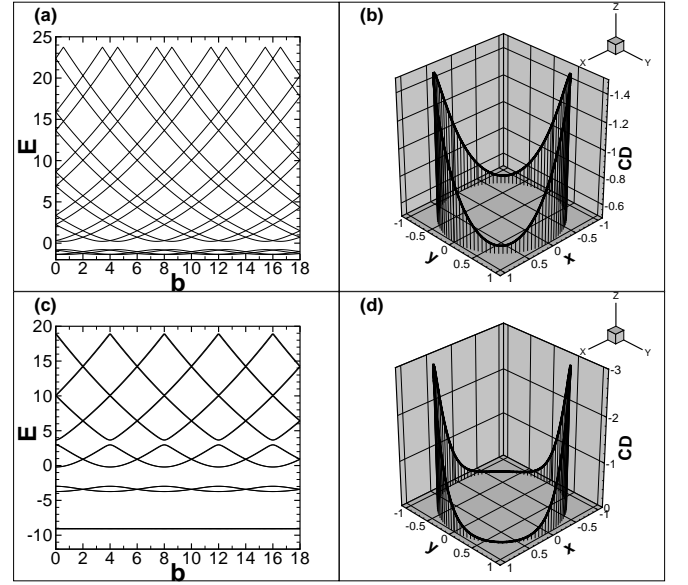


FIG. 9: (a) Energy spectrum of 1D ring while $\bar{\alpha} = 2$, $\bar{\beta} = 1$, $\bar{g} = 0$; (b) The charge density (CD) distribution of the lowest single electron state in a 1D ring while $\bar{\alpha} = 2$, $\bar{\beta} = 1$, $\bar{g} = 0$, $b = 0$; (c) Energy spectrum of 1D ring while $\bar{\alpha} = 4$, $\bar{\beta} = 3$, $\bar{g} = 0$; (d) The charge density (CD) distribution of the lowest single electron state in a 1D ring while $\bar{\alpha} = 4$, $\bar{\beta} = 3$, $\bar{g} = 0$, $b = 0$. The charge density is in units of $e/2\pi a$.

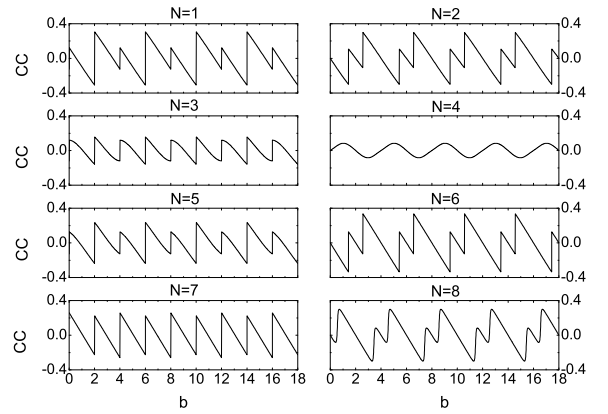


FIG. 10: The persistent CC in a 1D ring with different numbers of electrons N vs magnetic field b while $\bar{\alpha} = 2$, $\bar{\beta} = 1$, $\bar{g} = 0$. The persistent CC is in units of $2NE_0/\Phi_0$.

height, i.e., the product of the strengths of RSOI and DSOI (see Eq. (7)).

The persistent CC and SC are plotted in Fig. 10 and Fig. 11, respectively. We find that the oscillations of the persistent CC and SC become smooth and weak due to the gaps in the energy spectrum, especially when the Fermi level locates near the largest energy gap ($N = 4$). The persistent current (CC or SC) oscillation no longer consists of linear segments since the parabolic behavior of

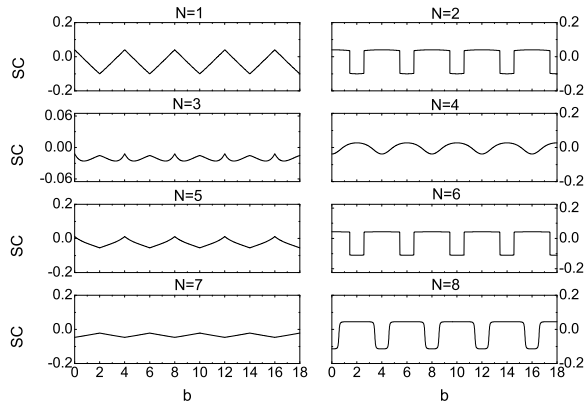


FIG. 11: Same as Fig. 10, but for the persistent SC. The persistent SC is in units of $NE_0/2\pi$.

the energy levels disappears due to the periodic potential $\frac{\bar{\alpha}\bar{\beta}}{2} \sin 2\varphi$ in the 1D Hamiltonian (see Eq. (7)).

The local spin orientation $S(\mathbf{r})$ also reveals the interplay between the RSOI and DSOI since $S(\mathbf{r})^R$ is quite different from $S(\mathbf{r})^D$. According to Eq. (7), the interplay between the RSOI and DSOI is divided into two parts, i.e., $\frac{\bar{\alpha}}{2}\sigma_r - \frac{\bar{\beta}}{2}\sigma_\varphi(-\varphi)$ in the kinetic term and the periodic potential $\frac{\bar{\alpha}\bar{\beta}}{2} \sin 2\varphi$. The first part makes the direction of the local spin orientation vary along the ring, and the second part leads to the electron localization (see Figs. 12(a) and 12(b)). When the SOI strengths increase, the spin orientation exhibits rapid variation due to the enhancement of the interplay between the RSOI and DSOI.

In Fig. 12(c), we plot the persistent SC as a function of RSOI strength $\bar{\alpha}$ and DSOI strength $\bar{\beta}$ for a fixed number of electrons $N = 8$ and magnetic field $b = 2$. The contour plot shows interesting symmetry. It is symmetric (anti-symmetric) with respect to the lines $\bar{\alpha} = 0$ and $\bar{\beta} = 0$ ($\bar{\alpha} = \pm\bar{\beta}$). From this figure we find that the maxima and minima of the persistent SC occur while only one of the two types of the SOI exists. That is because the effects of the RSOI and DSOI on spin splitting tend to cancel each other. The persistent SC becomes zero when the strengths of the RSOI and DSOI are equal to each other ($\bar{\alpha} = \pm\bar{\beta}$). This corresponds to the spin degenerate case discussed before. Besides the two orthogonal lines ($\bar{\alpha} = \pm\bar{\beta}$) on the $\bar{\alpha}$ - $\bar{\beta}$ plane there are many circle-like closed curves on which the persistent SC disappears. These zero-SC lines intersect the $\bar{\alpha}$ axis at those points $(\pm\sqrt{m^2-1}, 0)$ and the $\bar{\beta}$ axis at $(0, \pm\sqrt{m^2-1})$ where $m = 1, 2, 3, \dots$. The persistent SC disappears because the energy spectrum becomes degenerate again when the strengths of RSOI and DSOI are tuned to proper values even though they are not equal. The contour plot of the oscillation amplitude of the persistent CC for a fixed number of electrons $N = 8$ is shown in Fig. 12(d). The oscillation amplitude as a function of $\bar{\alpha}$ and $\bar{\beta}$ is

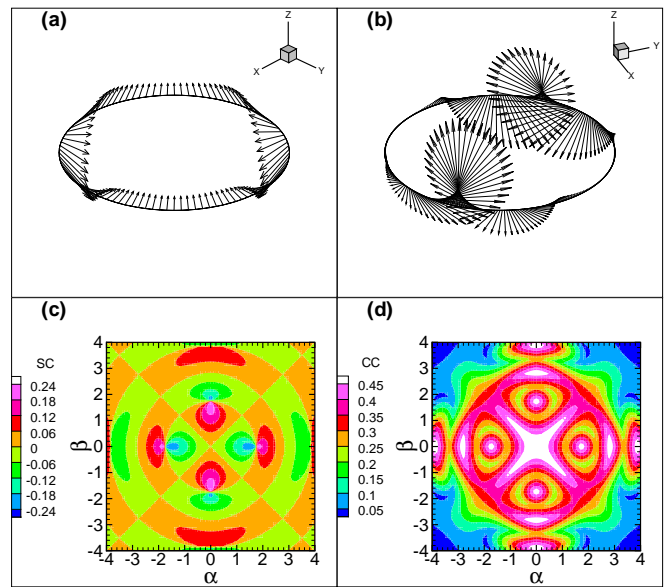


FIG. 12: (color online) (a) Local spin orientation $S(\mathbf{r})$ for the lowest spin-up level while $\bar{\alpha} = 2$, $\bar{\beta} = 1$, $\bar{g} = 0$, $b = 2$; (b) Local spin orientation $S(\mathbf{r})$ for the lowest spin-up level while $\bar{\alpha} = 4$, $\bar{\beta} = 3$, $\bar{g} = 0$, $b = 2$; (c) The persistent SC in a 1D ring with different RSOI and DSOI strengths when the magnetic field b is 2; (d) The oscillation amplitude of the persistent CC in a 1D ring with different RSOI and DSOI strengths. In Fig. 12(c) and Fig. 12(d) we set $\bar{g} = 0$ and $N = 8$. The persistent CC (SC) is in units of $2NE_0/\Phi_0$ ($NE_0/2\pi$).

symmetric with respect to the lines $\bar{\alpha} = 0$ and $\bar{\beta} = 0$ and $\bar{\alpha} = \pm\bar{\beta}$. When only one type of SOI appears, the maximum of the persistent CC oscillates with increased SOI strength. When both types of SOI are included, the maximum of the persistent CC decays since the interplay between the RSOI and DSOI leads to a periodic potential along the ring which results in the gaps in the energy spectrum, consequently smoothing and weakening the oscillation of the persistent CC.

E. Finite width effects

Now we turn to consider a mesoscopic ring with finite width. When a 2D ring is thin enough, its characteristics are almost the same as those of a 1D ring since the second radial levels are too high to be occupied and the compressing effect of the magnetic field on the radial wave function is negligible. Here we consider the wide ring case.

The energy spectrum for a 2D ring with a finite width while $\bar{\alpha} = 2$, $\bar{\beta} = 1$ and $\bar{g} = 0$ is plotted in Fig. 13(a). The second radial mode can be seen in the top of the energy spectrum. The compressing effect of the magnetic field on the radial wave function accounts for the increase of the energy with increasing magnetic fields. Like the 1D case, the interplay between the RSOI and DSOI leads to an effective periodic potential (see Eq. (A.2)), result-

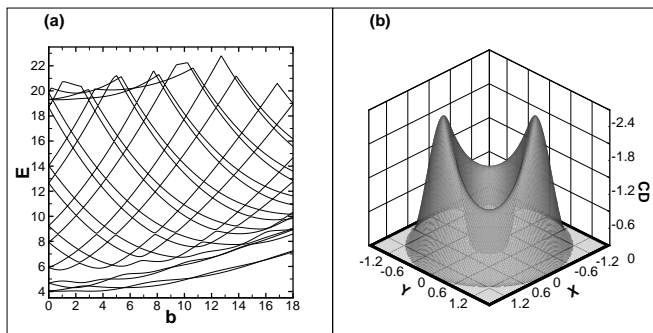


FIG. 13: (a) Energy spectrum for 2D hard wall ring with width $d = 1.33$ while $\bar{\alpha} = 2$, $\bar{\beta} = 1$, $\bar{g} = 0$; (b) The charge density (CD) distribution of the lowest single electron state in a 2D hard wall ring with $d = 1.33$ while $\bar{\alpha} = 2$, $\bar{\beta} = 1$, $\bar{g} = 0$, $b = 0$. The charge density is in units of $e/2\pi a^2$.

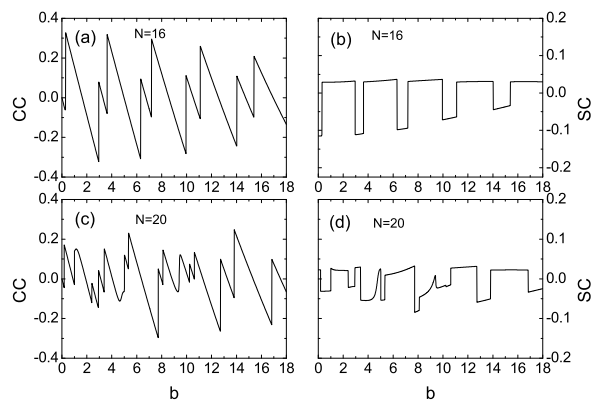


FIG. 14: (a) The persistent CC in a 2D ring *vs* magnetic field b while $\bar{\alpha} = 2$, $\bar{\beta} = 1$, $\bar{g} = 0$, the width $d = 1.33$ and $N = 16$; (b) Same as (a) but for the persistent SC; (c) Same as (a) except $N = 20$; (d) Same as (b) except $N = 20$. The persistent CC (SC) is in units of $2NE_0/\Phi_0$ ($NE_0/2\pi$).

ing in energy gaps that depend on the magnetic field. The charge density distribution of a single electron in a 2D ring at $b = 0$ is shown in Fig. 13(b). We find that the electron probability is localized due to the $\sin 2\varphi$ potential arising from the interplay between the RSOI and DSOI.

The persistent CC and SC in the 2D wide ring as a function of magnetic field are plotted in Fig. 14. The number of the electrons is tuned to detect the effect of the second radial mode. When we consider the contribution of the lowest 16 levels, the oscillations of the persistent CC and SC have a profile similar to that in the 1D ring because the second radial mode has not been involved yet. But when we increase the number of the electrons to 20, the quasi-periodicity of the persistent CC and SC as functions of the magnetic field b is destroyed. This feature arises from the contribution of the second radial mode.

IV. SUMMARY

We have conducted a theoretical investigation of the spin states and persistent CC and SC in mesoscopic rings with spin-orbit interactions. We have demonstrated theoretically that the Hamiltonian of the RSOI alone is mathematically equivalent to that of the DSOI alone by a unitary transformation T . This property results in the degenerate energy spectrum for equal strength RSOI and DSOI. The interplay between the RSOI and DSOI leads to an effective periodic potential $\frac{\bar{\alpha}\bar{\beta}}{2}\sin 2\varphi$. This periodic potential results in gaps in the energy spectrum, and smoothens and weakens the oscillations of the persistent CC and SC. The charge density and the local spin orientation $S(\mathbf{r})$ are localized along the ring due to the effect of the periodic potential. Higher radical modes become involved as the ring width increases, destroying the periodicity of the persistent CC and SC oscillations.

Acknowledgments

This work was supported by the NSFC Grant No. 60376016, 60525405.

APPENDIX: THE HAMILTONIAN AND AVAILABLE ANALYTICAL SOLUTIONS

The dimensionless Hamiltonian for a 2D ring reads

$$H_{2D} = H_k + H_R + H_D + H_Z + V(r), \quad (\text{A.1})$$

where the kinetic term $H_k = (\mathbf{e}_r k_r + \mathbf{e}_\varphi k_\varphi)^2$, the Rashba term $H_R = \bar{\alpha}(\sigma_r k_\varphi - \sigma_\varphi k_r)$, the Dresselhaus term $H_D = \bar{\beta}[\sigma_r(-\varphi)k_r - \sigma_\varphi(-\varphi)k_\varphi]$, and the Zeeman term $H_Z =$

$\bar{g}b\sigma_z/2$. $V(r)$ is the radial confining potential.

$$\begin{aligned}
H_{2D} &= -\frac{\partial^2}{\partial r^2} - \frac{1}{r} \frac{\partial}{\partial r} + V(r) + k_\varphi^2 \\
&+ [\bar{\alpha}\sigma_r - \bar{\beta}\sigma_\varphi(-\varphi)] k_\varphi \\
&+ \frac{i}{2r} [-\bar{\alpha}\sigma_\varphi + \bar{\beta}\sigma_r(-\varphi)] + \frac{1}{2}\bar{g}b\sigma_z \\
&+ \left(k_r - \frac{i}{2r}\right) [-\bar{\alpha}\sigma_\varphi + \bar{\beta}\sigma_r(-\varphi)] \\
&= -\frac{\partial^2}{\partial r^2} - \frac{1}{r} \frac{\partial}{\partial r} + V(r) \\
&+ \left(k_r - \frac{i}{2r}\right) [-\bar{\alpha}\sigma_\varphi + \bar{\beta}\sigma_r(-\varphi)] \\
&+ \left[k_\varphi + \frac{\bar{\alpha}}{2}\sigma_r - \frac{\bar{\beta}}{2}\sigma_\varphi(-\varphi)\right]^2 \\
&- \left[\frac{\bar{\alpha}}{2}\sigma_r - \frac{\bar{\beta}}{2}\sigma_\varphi(-\varphi)\right]^2 + \frac{1}{2}\bar{g}b\sigma_z \\
&= -\frac{\partial^2}{\partial r^2} - \frac{1}{r} \frac{\partial}{\partial r} + V(r) \\
&+ \left(k_r - \frac{i}{2r}\right) [-\bar{\alpha}\sigma_\varphi + \bar{\beta}\sigma_r(-\varphi)] \\
&+ \left[k_\varphi + \frac{\bar{\alpha}}{2}\sigma_r - \frac{\bar{\beta}}{2}\sigma_\varphi(-\varphi)\right]^2 \\
&- \frac{\bar{\alpha}^2 + \bar{\beta}^2}{4} + \frac{\bar{\alpha}\bar{\beta}}{2} \sin 2\varphi + \frac{1}{2}\bar{g}b\sigma_z. \quad (\text{A.2})
\end{aligned}$$

Specifically we write $H_{2D} = H_0 + H_1$, where $H_0 = -\frac{\partial^2}{\partial r^2} - \frac{1}{r} \frac{\partial}{\partial r} + V(r)$. The correct 1D Hamiltonian H can be obtained by evaluating the expectation of H_1 in the lowest radial mode of H_0 .²³ In the limit of a very narrow ring, we can set r to be a constant value ($r = 1$) and the following equation will hold for an arbitrarily given confining potential $V(r)$:

$$\langle \rho_0 | \frac{\partial}{\partial r} + \frac{1}{2r} | \rho_0 \rangle = 0. \quad (\text{A.3})$$

Here ρ_0 is the lowest radial mode for $V(r)$. Now we can write the 1D Hamiltonian explicitly. We get

$$\begin{aligned}
H &= \left[-i \frac{\partial}{\partial \varphi} + \frac{b}{4} + \frac{\bar{\alpha}}{2}\sigma_r - \frac{\bar{\beta}}{2}\sigma_\varphi(-\varphi)\right]^2 \\
&- \frac{\bar{\alpha}^2 + \bar{\beta}^2}{4} + \frac{\bar{\alpha}\bar{\beta}}{2} \sin 2\varphi + \frac{1}{2}\bar{g}b\sigma_z. \quad (\text{A.4})
\end{aligned}$$

A unitary operator $T = \begin{bmatrix} 0 & \exp[-i\pi/4] \\ -\exp[i\pi/4] & 0 \end{bmatrix}$ is defined, and we have $T^\dagger = T^{-1} = -T$. By applying this unitary operator, the Hamiltonian becomes

$$\begin{aligned}
THT^\dagger &= \left[-i \frac{\partial}{\partial \varphi} + \frac{b}{4} + \frac{\bar{\beta}}{2}\sigma_r - \frac{\bar{\alpha}}{2}\sigma_\varphi(-\varphi)\right]^2 \\
&- \frac{\bar{\alpha}^2 + \bar{\beta}^2}{4} + \frac{\bar{\alpha}\bar{\beta}}{2} \sin 2\varphi - \frac{1}{2}\bar{g}b\sigma_z. \quad (\text{A.5})
\end{aligned}$$

Thus the Hamiltonian in which $\bar{\alpha} = a$, $\bar{\beta} = b$, $\bar{g} = c$ is mathematically equivalent to that in which $\bar{\alpha} = b$, $\bar{\beta} = a$, $\bar{g} = -c$.

The Hamiltonian in matrix form is

$$\begin{aligned}
H &= \begin{bmatrix} H_{11} & H_{12} \\ H_{21} & H_{22} \end{bmatrix}, \text{ where} \\
H_{11} &= \left(-i \frac{\partial}{\partial \varphi} + \frac{b}{4}\right)^2 + \bar{g}b/2, \\
H_{12} &= \bar{\alpha}e^{-i\varphi} \left(-i \frac{\partial}{\partial \varphi} + \frac{b}{4} - \frac{1}{2}\right) + i\bar{\beta}e^{i\varphi} \left(-i \frac{\partial}{\partial \varphi} + \frac{b}{4} + \frac{1}{2}\right), \\
H_{21} &= \bar{\alpha}e^{i\varphi} \left(-i \frac{\partial}{\partial \varphi} + \frac{b}{4} + \frac{1}{2}\right) - i\bar{\beta}e^{-i\varphi} \left(-i \frac{\partial}{\partial \varphi} + \frac{b}{4} - \frac{1}{2}\right), \\
H_{22} &= \left(-i \frac{\partial}{\partial \varphi} + \frac{b}{4}\right)^2 - \bar{g}b/2. \quad (\text{A.6})
\end{aligned}$$

To solve the equation $H\Psi = E\Psi$, we expand the wavefunction Ψ as $\Psi = \begin{pmatrix} \Psi_1 \\ \Psi_2 \end{pmatrix} = \sum_m \begin{pmatrix} a_m \\ b_m \end{pmatrix} \Theta_m(\varphi)$, where $\Theta_m(\varphi) = \frac{1}{\sqrt{2\pi}} \exp[im\varphi]$. The secular equation becomes

$$\begin{cases} b_{m+1}\bar{\alpha}(m + \frac{b}{4} + \frac{1}{2}) + ib_{m-1}\bar{\beta}(m + \frac{b}{4} - \frac{1}{2}) \\ = [E - (m + \frac{b}{4})^2 - \bar{g}b/2] a_m \\ a_{m-1}\bar{\alpha}(m + \frac{b}{4} - \frac{1}{2}) - ia_{m+1}\bar{\beta}(m + \frac{b}{4} + \frac{1}{2}) \\ = [E - (m + \frac{b}{4})^2 + \bar{g}b/2] b_m \end{cases} \cdot (\text{A.7})$$

Generally, we can write the Hamiltonian in an infinite quintuple diagonal matrix form based on Eq. (A.7).

$$\begin{bmatrix}
\ddots & & & & & & & & \\
\ddots & (\frac{b}{4}-1)^2 + \frac{\bar{g}b}{2} & 0 & & & 0 & 0 & 0 & 0 \\
0 & 0 & (\frac{b}{4}-1)^2 - \frac{\bar{g}b}{2} & -i\bar{\beta}(\frac{b}{4}-\frac{1}{2}) & & 0 & 0 & 0 & 0 \\
\ddots & 0 & i\bar{\beta}(\frac{b}{4}-\frac{1}{2}) & (\frac{b}{4})^2 + \frac{\bar{g}b}{2} & & 0 & 0 & \bar{\alpha}(\frac{b}{4}+\frac{1}{2}) & 0 \\
0 & \bar{\alpha}(\frac{b}{4}-\frac{1}{2}) & 0 & 0 & & (\frac{b}{4})^2 - \frac{\bar{g}b}{2} & -i\bar{\beta}(\frac{b}{4}+\frac{1}{2}) & 0 & \ddots \\
0 & 0 & 0 & 0 & & i\bar{\beta}(\frac{b}{4}+\frac{1}{2}) & (\frac{b}{4}+1)^2 + \frac{\bar{g}b}{2} & 0 & 0 \\
0 & 0 & 0 & \bar{\alpha}(\frac{b}{4}+\frac{1}{2}) & & 0 & 0 & (\frac{b}{4}+1)^2 - \frac{\bar{g}b}{2} & \ddots \\
0 & 0 & 0 & 0 & & \ddots & 0 & \ddots & \ddots
\end{bmatrix}
\begin{bmatrix}
\vdots \\
a_{-1} \\
b_{-1} \\
a_0 \\
b_0 \\
a_1 \\
b_1 \\
\vdots
\end{bmatrix}
= E
\begin{bmatrix}
\vdots \\
a_{-1} \\
b_{-1} \\
a_0 \\
b_0 \\
a_1 \\
b_1 \\
\vdots
\end{bmatrix}. \tag{A.8}$$

We consider three different cases. For the first and second cases, in which the quintuple diagonal matrices are reducible, analytical solutions can be obtained.

a) $\bar{\alpha} \neq 0, \bar{\beta} = 0$;

$$\begin{bmatrix}
(m+b/4)^2 + \bar{g}b/2 & \bar{\alpha}(m+b/4+1/2) \\
\bar{\alpha}(m+b/4+1/2) & (m+b/4+1)^2 - \bar{g}b/2
\end{bmatrix}
\begin{bmatrix}
a_m \\
b_{m+1}
\end{bmatrix}
= E
\begin{bmatrix}
a_m \\
b_{m+1}
\end{bmatrix}. \tag{A.9}$$

The eigenvalues are

$$E_{n,\sigma}^R = \left(n + \frac{b}{4} + \frac{\sigma}{2} - \frac{\sigma}{2 \cos \theta_{n,\sigma}} \right)^2 - \frac{\tan^2 \theta_{n,\sigma}}{4} + \sigma \frac{\bar{g}b}{2 \cos \theta_{n,\sigma}}, \tag{A.10}$$

where $\tan \theta_{n,\sigma} = \frac{\bar{\alpha}(n+b/4+\sigma/2)}{n+b/4+\sigma/2-\bar{g}b/2}$. The corresponding eigenvectors are

$$\Psi_{n,\uparrow}^R = \frac{1}{\sqrt{2\pi}} e^{i(n+1/2)\varphi} \begin{pmatrix} \cos \frac{\theta_{n,\uparrow}}{2} e^{-i\varphi/2} \\ -\sin \frac{\theta_{n,\uparrow}}{2} e^{i\varphi/2} \end{pmatrix} \tag{A.11}$$

and

$$\Psi_{n,\downarrow}^R = \frac{1}{\sqrt{2\pi}} e^{i(n-1/2)\varphi} \begin{pmatrix} \sin \frac{\theta_{n,\downarrow}}{2} e^{-i\varphi/2} \\ \cos \frac{\theta_{n,\downarrow}}{2} e^{i\varphi/2} \end{pmatrix}. \tag{A.12}$$

The local spin orientations for eigenstates are

$$\begin{aligned}
& S(\mathbf{r})_{n,\uparrow}^R \\
&= \frac{\hbar}{4\pi a} [\sin(-\theta_{n,\uparrow})(\cos \varphi \mathbf{e}_x + \sin \varphi \mathbf{e}_y) + \cos(-\theta_{n,\uparrow})\mathbf{e}_z]
\end{aligned} \tag{A.13}$$

and

$$\begin{aligned}
& S(\mathbf{r})_{n,\downarrow}^R \\
&= \frac{\hbar}{4\pi a} [\sin(\pi - \theta_{n,\downarrow})(\cos \varphi \mathbf{e}_x + \sin \varphi \mathbf{e}_y) + \cos(\pi - \theta_{n,\downarrow})\mathbf{e}_z].
\end{aligned} \tag{A.14}$$

b) $\bar{\alpha} = 0, \bar{\beta} \neq 0$;

$$\begin{bmatrix}
(m+b/4+1)^2 + \bar{g}b/2 & i\bar{\beta}(m+b/4+1/2) \\
-i\bar{\beta}(m+b/4+1/2) & (m+b/4)^2 - \bar{g}b/2
\end{bmatrix}
\begin{bmatrix}
a_{m+1} \\
b_m
\end{bmatrix}
= E
\begin{bmatrix}
a_{m+1} \\
b_m
\end{bmatrix}. \tag{A.15}$$

The eigenvalues are

$$E_{n,\sigma}^D = \left(n + \frac{b}{4} - \frac{\sigma}{2} + \frac{\sigma}{2 \cos \eta_{n,\sigma}} \right)^2 - \frac{\tan^2 \eta_{n,\sigma}}{4} + \sigma \frac{\bar{g}b}{2 \cos \eta_{n,\sigma}}, \tag{A.16}$$

where $\tan \eta_{n,\sigma} = \frac{\bar{\beta}(n+b/4-\sigma/2)}{n+b/4-\sigma/2+\bar{g}b/2}$. The corresponding eigenvectors are

$$\Psi_{n,\uparrow}^D = \frac{1}{\sqrt{2\pi}} e^{i(n-1/2)\varphi} \begin{pmatrix} \cos \frac{\eta_{n,\uparrow}}{2} e^{i\varphi/2} \\ -i \sin \frac{\eta_{n,\uparrow}}{2} e^{-i\varphi/2} \end{pmatrix} \tag{A.17}$$

and

$$\Psi_{n,\downarrow}^D = \frac{1}{\sqrt{2\pi}} e^{i(n+1/2)\varphi} \begin{pmatrix} -i \sin \frac{\eta_{n,\downarrow}}{2} e^{i\varphi/2} \\ \cos \frac{\eta_{n,\downarrow}}{2} e^{-i\varphi/2} \end{pmatrix}. \tag{A.18}$$

The local spin orientations for the eigenstates are

$$\begin{aligned}
 S(\mathbf{r})_{n,\uparrow}^D & \\
 &= \frac{\hbar}{4\pi a} [\sin(-\eta_{n,\uparrow})(\sin \varphi \mathbf{e}_x + \cos \varphi \mathbf{e}_y) + \cos(-\eta_{n,\uparrow})\mathbf{e}_z]
 \end{aligned}
 \tag{A.19}$$

and

$$\begin{aligned}
 S(\mathbf{r})_{n,\downarrow}^D & \\
 &= \frac{\hbar}{4\pi a} [\sin(\pi - \eta_{n,\downarrow})(\sin \varphi \mathbf{e}_x + \cos \varphi \mathbf{e}_y) + \cos(\pi - \eta_{n,\downarrow})\mathbf{e}_z].
 \end{aligned}
 \tag{A.20}$$

c) $\bar{\alpha} \neq 0, \bar{\beta} \neq 0$.

While both RSOI and DSOI have nonvanishing strengths, we cannot reduce the infinite quintuple diagonal matrix shown in Eq. (A.8) into a more compact form. Thus analytical solutions do not exist. We give numerical results instead.

* Author to whom correspondence should be addressed.
Electronic address: kchang@red.semi.ac.cn

- ¹ S. A. Wolf, D. D. Awschalom, R. A. Buhrman, J. M. Daughton, S. von Molnár, M. L. Roukes, A. Y. Chtchelkanova, and D. M. Treger, *Science* **294**, 1488 (2001).
- ² E. Tsitsishvili, G. S. Lozano, and A. O. Gogolin, *Phys. Rev. B* **70**, 115316 (2004).
- ³ G. Dresselhaus, *Phys. Rev.* **100**, 580 (1955).
- ⁴ E. I. Rashba, *Sov. Phys. Solid State* **2**, 1109 (1960).
- ⁵ Y. A. Bychkov and E. I. Rashba, *J. Phys. C* **17**, 6039 (1984).
- ⁶ S. Murakami, N. Nagaosa, and S. C. Zhang, *Science* **301**, 1348 (2003).
- ⁷ J. Sinova, D. Culcer, Q. Niu, N. A. Sinitsyn, T. Jungwirth, and A. H. MacDonald, *Phys. Rev. Lett.* **92**, 126603 (2004).
- ⁸ A. Fuhrer, S. Lüscher, T. Ihn, T. Heinzl, K. Ensslin, W. Wegscheider, and M. Bichler, *Nature* **413**, 822 (2001).
- ⁹ M. Büttiker, Y. Imry, and R. Landauer, *Phys. Lett.* **96A**, 365 (1983).
- ¹⁰ L. Wendler, V. M. Fomin, and A. A. Krokhin, *Phys. Rev. B* **50**, 4642 (1994).
- ¹¹ T. Chakraborty and P. Pietiläinen, *Phys. Rev. B* **50**, 8460 (1994).
- ¹² V. Chandrasekhar, R. A. Webb, M. J. Brady, M. B. Ketchen, W. J. Gallagher, and A. Kleinsasser, *Phys. Rev. Lett.* **67**, 3578 (1991).
- ¹³ D. Mailly, C. Chapelier, and A. Benoit, *Phys. Rev. Lett.* **70**, 2020 (1993).
- ¹⁴ F. Meier and D. Loss, *Phys. Rev. Lett.* **90**, 167204 (2003).
- ¹⁵ F. Schütz, M. Kollar, and P. Kopietz, *Phys. Rev. Lett.* **91**,

- 017205 (2003).
- ¹⁶ J. Spletstoesser, M. Governale, and U. Zülicke, *Phys. Rev. B* **68**, 165341 (2003).
- ¹⁷ B. Molnár, F. M. Peeters, and P. Vasilopoulos, *Phys. Rev. B* **69**, 155335 (2004).
- ¹⁸ S. Souma and B. K. Nikolić, *Phys. Rev. Lett.* **94**, 106602 (2005).
- ¹⁹ G. Lommer, F. Malcher, and U. Rössler, *Phys. Rev. Lett.* **60**, 728 (1988).
- ²⁰ S. D. Ganichev, V. V. Bel'kov, L. E. Golub, E. L. Ivchenko, P. Schneider, S. Giglberger, J. Eroms, J. De Boeck, G. Borghs, W. Wegscheider, et al., *Phys. Rev. Lett.* **92**, 256601 (2004).
- ²¹ M. C. Chang, *Phys. Rev. B* **71**, 085315 (2005).
- ²² W. Yang and K. Chang, *Phys. Rev. B* **73**, 045303 (2006).
- ²³ F. E. Meijer, A. F. Morpurgo, and T. M. Klapwijk, *Phys. Rev. B* **66**, 033107 (2002).
- ²⁴ T. Chakraborty, in *Adv. in Solid State Phys.*, edited by B. Kramer (Springer-Verlag, Berlin Heidelberg, 2003), vol. **43**, pp. 79–94.
- ²⁵ G. S. Lozano and M. J. Sánchez, *Phys. Rev. B* **72**, 205315 (2005).
- ²⁶ O. Madelung, ed., *Physics of Group IV Elements and III-V Compounds*, Landolt-Börnstein (New Series) Group III Condensed Matter Vol. **17**, Pt. a (Springer-Verlag, Berlin, 1982).
- ²⁷ I. S. Gradshteyn and I. M. Ryzhik, eds., *Tables of Integrals, Series, and Products* (Academic Press, New York, 1980).